International Journal of Electrical and Power Engineering 2 (5): 353-364, 2008
ISSN: 1990-7958

Performances Study of the DFIG Associated to the Variable Speed Wind Turbine Connected to the Grid

S. Taraft, D. Rekioua and D. Aouzellag
Department of Electrical Engineering, A/MIRA University, 06000 Bejaia, Algeria

Abstract: The aim of this research is the study of the performances of the Doubly Fed Induction Generator (DFIG) in a wind turbine of high level powers at variable speed, connected to the electrical grid. The stator of the DFIG is directly connected to the grid, the rotor is connected to the grid fed by a direct frequency converter (called matrix converter). The control of the powers transit (active and reactive) between the aerogenerator and the grid is carried out by the adjustment of the rotor sizes of the DFIG. In a first part, the modeling of the various parts of the aerogenerator is presented. The Maximum Power Point Tracking (MPPT) algorithm to maximize the generated power is used. In a second part, the principle of powers control exchanged between the wind system and the grid is exposed. Finally, the simulation results of the dynamic behavior of the studied system are presented to justify the reliability of the model suggested and the order applied.

Key words: Wind turbine, DFIG, variable speed, matrix converter, power control, MPPT

INTRODUCTION

The application of the DFIG in the modern wind tubine becomes an imposing reality, by the performances which it can offer. Indeed, it allows an operation out of generator in the 2 quadrants torque-speed (Chang, 2002). Generally, if a wind turbine containing the DFIG, the stator is connected directly to the grid; the rotor is connected to the grid by the means of a static converter (Robyns and Nasser, 2001). Being given that the power brought into play in the rotor circuit remains lower than that of the stator circuit; the constraints on the static converter will be decreased, which leads to the reduction of the size and the cost of the converter (Poitier, 2003).

The direct converter is proposed to substitute the conventional converter (cascade rectifier-inverter) in the purpose of improving the performances of the wind turbine. The Matrix Converter (MC) eliminates the dc-link filter elements and thus resolves the size, weight and reliability issues and also provides an option for the design of the converter as a compact/modular unit (Han, 2004).

The control of the rotor sizes of the DFIG allows the management of the transit of powers between the aerogenerator and the grid (Ghedamsi *et al*., 2006).

The synoptic diagram of the studied system is represented by Fig. 1.

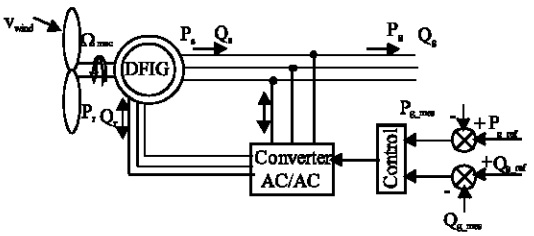

Fig. 1: Power contorl between the DFIG and the grid

MODELLING OF THE AEROGENERATOR

Modelling of the mechanical part: The total kinetic power of the wind through a wind disc of radius R, is given by the following relation (Chang, 2002).

$$P_{wind} = \frac{1}{2}\rho\pi.R^2.v_{wind}^3 \quad (1)$$

The aerodynamic power, which is converted by a wind turbine, P_t is dependent on the power coefficient C_p. It is given by:

$$P_t = \frac{1}{2}C_p(\lambda).\rho.\pi.R^2.v_{wind}^3 \quad (2)$$

ρ represent the air density and v_{wind} the wind velocity.

Corresponding Author: S. Taraft, Department of Electrical Engineering, A/MIRA University, 06000 Bejaia, Algeria

A wind turbine can only convert just a certain percentage of the captured wind power. This percentage is represented by $C_p(\lambda)$ which is function of the wind speed, turbine speed and the pith angle of specific wind turbine blades (El Aimani, 2003; Chang, 2002).

Although, this equation seems simple, C_p is dependent on the ratio λ between the turbine angular velocity Ω_t and the wind speed v_{wind}. This ratio is called the tip speed ratio

$$\begin{cases} \lambda = \dfrac{\Omega_t . R}{v_{wind}} \\ \Omega_t = \dfrac{\Omega_{mec}}{G} \end{cases} \quad (3)$$

A typical relationship between C_p and λ is shown in Fig. 2.

We can show in this figure the value of λ for which C_p is maximum and that maximise the power for a given wind speed. The peak power for each wind speed occurs at the point where C_p is maximised. To maximise the generated power, it is therefore desirable for the generator to have a power characteristic that will follow the maximum C_{p_max} line.

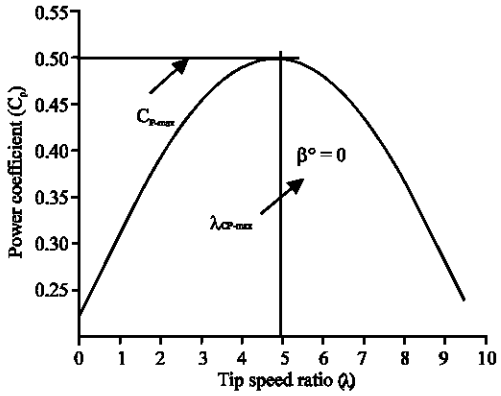

Fig. 2: Power coefficient for the wind turbine model

The action of the speed corrector must achieve 2 tasks (Poitiers *et al.*, N.D).

- It must control the mechanical speed Ω_{mec} in order to get a speed reference Ω_{mec_ref}.
- It must attenuate the action of the aerodynamic torque, which is an input disturbance.

The simplified representation in the form of diagram blocks is given in Fig. 3.

The aerodynamic torque is defined as the relationship between the aerodynamic power and the angular velocity of the turbine

$$T_{aero} = \frac{P_{aero}}{\Omega_t} \quad (4)$$

The machine torque shaft is given by:

$$T_{tree} = \frac{T_{aero}}{G} \quad (5)$$

The mechanical speed evolution is determined from the total torque T_{mec} applied to the rotor

$$J \frac{d\Omega_{mec}}{dt} = T_{mec} \quad (6)$$

$$T_{mec} = T_{tree} - T_{em} - T_{visq} \quad (7)$$

The torque resist due to frictions T_{visq} is modelled by a coefficient of viscous frictions f:

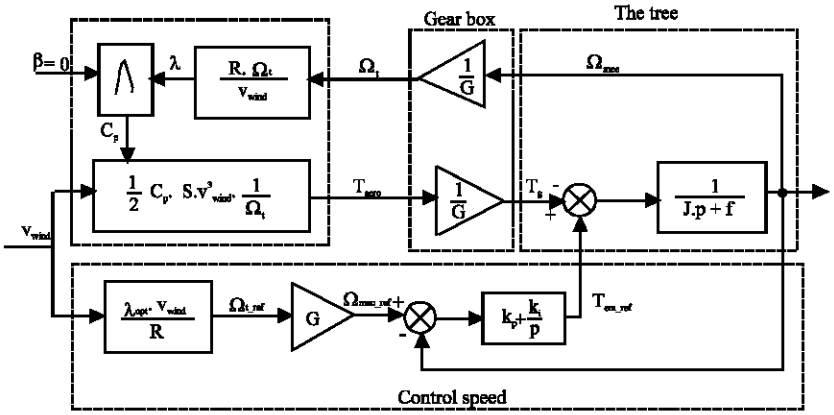

Fig. 3: Device control with control speed

$$T_{visq} = f.\Omega_{mec} \tag{8}$$

The expression of the optimal mechanical power $P_{mec\text{-}opt}$ is obtained as follows.

$$P_{mec\_opt} = \frac{1}{2}\frac{C_{P_{max}}.\rho.\pi.R^5}{G^3.\lambda_{opt}^3}.\Omega_{mec}^3 \tag{9}$$

The DFIG modelling: The DFIG dynamic model in Park's reference is expressed as follows (Poitier, 2003).
Electric equations

$$\begin{cases} v_{ds} = R_s i_{ds} + \dfrac{d}{dt}\varphi_{ds} - \omega_s \varphi_{qs} \\ v_{qs} = R_s i_{qs} + \dfrac{d}{dt}\varphi_{qs} + \omega_s \varphi_{ds} \\ v_{dr} = R_r i_{dr} + \dfrac{d}{dt}\varphi_{dr} - (\omega_s - \omega)\varphi_{qr} \\ v_{qr} = R_r i_{qr} + \dfrac{d}{dt}\varphi_{qr} + (\omega_s - \omega)\varphi_{dr} \end{cases} \tag{10}$$

$$\begin{cases} \varphi_{ds} = L_s i_{ds} + L_m i_{dr} \\ \varphi_{qs} = L_s i_{qs} + L_m i_{qr} \\ \varphi_{dr} = L_r i_{dr} + L_m i_{ds} \\ \varphi_{qr} = L_r i_{qr} + L_m i_{qs} \end{cases} \tag{11}$$

Electromagnetic torque equation

$$T_{em} = p(\varphi_{ds}.i_{qs} - \varphi_{qs}.i_{ds}) \tag{12}$$

The active and reactive stator and rotor powers are given by:

$$\begin{cases} P_s = v_{ds}.i_{ds} + v_{qs}.i_{qs} \\ Q_s = v_{qs}.i_{ds} - v_{ds}.i_{qs} \\ P_r = v_{dr}.i_{dr} + v_{qr}.i_{qr} \\ Q_r = v_{qr}.i_{dr} - v_{dr}.i_{qr} \end{cases} \tag{13}$$

And the powers exchanged between the system and the grid are expressed by:

$$\begin{cases} P_g = P_s + P_r \\ Q_g = Q_s + Q_r \end{cases} \tag{14}$$

MODELLING OF THE MATRIX CONVERTER

The simplified three phases- three phases matrix converter topology incorporated in system of wind turbine is shown in Fig. 4. Matrix converter consists, of nine bidirectional switches and each output phase is associated with three switches set connected to three input phases. This configuration of bidirectional switch enables to connect any of input phase a, b or c to any of output phase A, B or C at any instant. Since the matrix converter is supplied by the voltage source, the input phases must not be shorted and due to the inductive nature of the load, the output phases must not be open. If the switch function of a switch S_{ij} in Fig. 5 is defined as:

$$S_{ij}(t) = \begin{cases} 1 & S_{ij} \text{ is close} \\ 0 & S_{ij} \text{ is opened} \end{cases} \quad i \in \{a, b, c\},\ j \in \{A, B, C\} \tag{15}$$

The constraints can be expressed as:

$$\begin{cases} S_{aj} + S_{bj} + S_{cj} = 1 \\ j \in \{A, B, C\} \end{cases} \tag{16}$$

Modulation strategy: The object of the modulation strategy is to synthesize the output voltages from the input voltages and the input currents from the output currents. The three phase matrix converter can be represented by a 3 by 3 matrix from because the nine bidirectional switches can connect one input phase to one output phase directly without any intermediate energy storage elements. Therefore, the output voltage and input currents of the matrix converter can be represented by the transfer functionT and the transposed T^T such as.

$$v_s = T \times v_i \tag{17}$$

$$\begin{bmatrix} v_A \\ v_B \\ v_C \end{bmatrix} = \begin{bmatrix} S_{aA} & S_{bA} & S_{cA} \\ S_{aB} & S_{bB} & S_{cB} \\ S_{aC} & S_{bC} & S_{cC} \end{bmatrix}.\begin{bmatrix} v_a \\ v_b \\ v_c \end{bmatrix} \tag{18}$$

$$i_i = T^T \times i_s \tag{19}$$

Defining modulation strategy is actually filling in the elements of the transfer matrix. Although, several modulation strategies have been proposed (Chang, 2002). The equivalent circuit of the indirect modulation is shown in Fig 5.

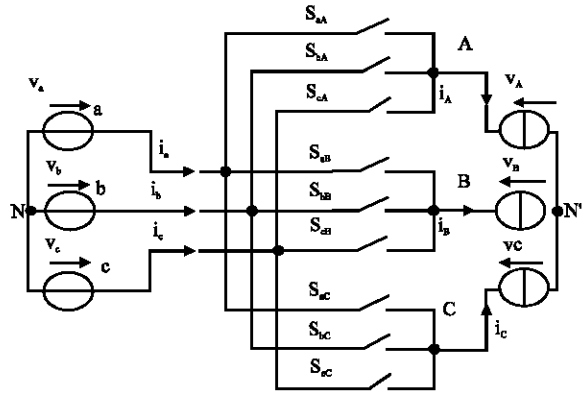

Fig. 4: Matrix converter topology

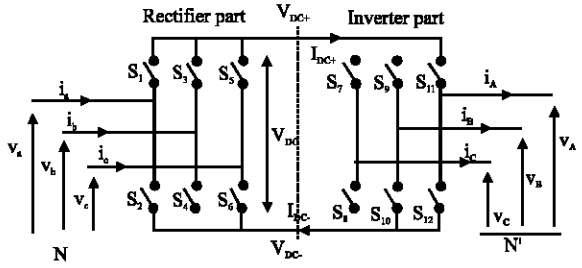

Fig. 5: Matrix converter model with the fictive Dc-link voltage

The basic idea of the indirect modulation technique is to decouple the control of the input currents and output voltage. The transfer function T for the matrix converter Eq. (18) into the product of the rectifier transfer function and inverter transfer function.

$$T = R * I$$

$$\begin{bmatrix} S_{aA} & S_{aB} & S_{aC} \\ S_{bA} & S_{bB} & S_{bC} \\ S_{cA} & S_{cB} & S_{cC} \end{bmatrix} = \begin{bmatrix} S_7 & S_8 \\ S_9 & S_{10} \\ S_{11} & S_{12} \end{bmatrix} \cdot \begin{bmatrix} S_1 & S_3 & S_5 \\ S_2 & S_4 & S_6 \end{bmatrix} \quad (20)$$

This way to modelize the matrix converter provides the basis to regard the matrix converter as a buck-to-buck PWM converter without any Dc-link energy storage. This means the well know space vector PWM strategies for voltage source inverter (VSI) or PWM rectifier can be applied to the matrix converter.

By substituting Eq. (20) into Eq. (18).

$$\begin{bmatrix} v_A \\ v_B \\ v_C \end{bmatrix} = \begin{bmatrix} S_7 & S_8 \\ S_9 & S_{10} \\ S_{11} & S_{12} \end{bmatrix} \cdot \begin{bmatrix} S_1 & S_3 & S_5 \\ S_2 & S_4 & S_6 \end{bmatrix} \cdot \begin{bmatrix} v_a \\ v_b \\ v_c \end{bmatrix} \quad (21)$$

$$\begin{bmatrix} v_A \\ v_B \\ v_C \end{bmatrix} = \begin{bmatrix} S_7.S_1 + S_8.S_2 & S_7.S_3 + S_8.S_4 & S_7.S_5 + S_8.S_6 \\ S_9.S_1 + S_{10}.S_2 & S_9.S_3 + S_{10}.S_4 & S_9.S_5 + S_{10}.S_6 \\ S_{11}.S_1 + S_{12}.S_2 & S_{11}.S_3 + S_{12}.S_4 & S_{11}.S_5 + S_{12}.S_6 \end{bmatrix} \cdot \begin{bmatrix} v_a \\ v_b \\ v_c \end{bmatrix} \quad (22)$$

Therefore, the indirect modulation technique enables well-known space vector PWM to be applied for a rectifier as well as an inverter stage (Chang, 2002).

In what follows we describe two independent space vector modulations for current source rectifier and voltage source inverter stages and then the two modulation results are combined to a modulation for the matrix converter.

Space vector modulation for the rectifier stage: From Fig 5, it is seen that a virtual Dc-link is established. In the indirect space vector modulation, all quantities are referred to this virtual Dc-link. The input currents and dc-link voltage can be found from the switch states as seen in Eq. (23) and (24).

$$\begin{bmatrix} i_a \\ i_b \\ i_c \end{bmatrix} = \begin{bmatrix} S_1 & S_2 \\ S_3 & S_4 \\ S_5 & S_6 \end{bmatrix} \cdot \begin{bmatrix} I_{DC+} \\ I_{DC-} \end{bmatrix} \quad (23)$$

$$\begin{bmatrix} V_{DC+} \\ V_{DC-} \end{bmatrix} = \begin{bmatrix} S_1 & S_3 & S_5 \\ S_2 & S_4 & S_6 \end{bmatrix} \cdot \begin{bmatrix} v_A \\ v_B \\ v_C \end{bmatrix} \quad (24)$$

The possible switch combinations of the rectifier are shown in Table 1 and the space vector hexagon is seen in Fig. 6. For one such set of vectors the span is shown on Fig. 7 where also the vector lengths are shown. The duty cycles for the adjacent vectors on Fig. 7 can be calculated using Eq. (25)

$$\begin{cases} d_\gamma = m_C.\sin\left(\frac{\pi}{3} - \theta_C\right) = T_\gamma / T_S \\ d_\delta = m_C.\sin(\theta_C) = T_\delta / T_\delta \\ d_{0C} = 1 - d_\gamma + d_\delta = T_{0C} / T_S \end{cases} \quad (25)$$

$$0 \le m_C \le 1$$

$$m_C = \frac{I_I^*}{I_{DC}}$$

Table 1: Switch states and generated vectors for the rectifier

Type	Vecteurs	$\begin{bmatrix} S_1 & S_3 & S_5 \\ S_2 & S_4 & S_7 \end{bmatrix}^T$	i_a	i_b	i_c	$\|I_i\|$	$<I_i$	V_{DC}
Actifs	I_1[ab]	$\begin{bmatrix} 1 & 0 & 0 \\ 0 & 1 & 0 \end{bmatrix}^T$	I_{DC+}	I_{DC-}	0	$\frac{2}{\sqrt{3}} I_{DC}$	$-\frac{\pi}{6}$	v_{ab}
	I_2[ac]	$\begin{bmatrix} 1 & 0 & 0 \\ 0 & 0 & 1 \end{bmatrix}^T$	I_{DC+}	0	I_{DC-}	$\frac{2}{\sqrt{3}} I_{DC}$	$\frac{\pi}{6}$	$-v_{ac}$
	I_3[bc]	$\begin{bmatrix} 0 & 1 & 0 \\ 0 & 0 & 1 \end{bmatrix}^T$	0	I_{DC+}	I_{DC-}	$\frac{2}{\sqrt{3}} I_{DC}$	$\frac{\pi}{2}$	v_{bc}
	I_4[ba]	$\begin{bmatrix} 0 & 1 & 0 \\ 1 & 0 & 0 \end{bmatrix}^T$	I_{DC-}	I_{DC-}	I_{DC+}	$\frac{2}{\sqrt{3}} I_{DC}$	$\frac{5\pi}{6}$	$-v_{ba}$
	I_5[ca]	$\begin{bmatrix} 0 & 0 & 1 \\ 1 & 0 & 0 \end{bmatrix}^T$	I_{DC-}	0	I_{DC+}	$\frac{2}{\sqrt{3}} I_{DC}$	$-\frac{5\pi}{6}$	v_{ca}
	I_6[cb]	$\begin{bmatrix} 0 & 0 & 1 \\ 0 & 1 & 0 \end{bmatrix}^T$	0	I_{DC-}	I_{DC+}	$\frac{2}{\sqrt{3}} I_{DC}$	$-\frac{\pi}{2}$	$-v_{cb}$
Nuls	I_0[aa][bb][cc]	$\begin{bmatrix} 1 & 0 & 0 \\ 1 & 0 & 0 \end{bmatrix}^T \begin{bmatrix} 0 & 1 & 0 \\ 0 & 1 & 0 \end{bmatrix}^T \begin{bmatrix} 0 & 0 & 1 \\ 0 & 0 & 1 \end{bmatrix}^T$				0	0	0

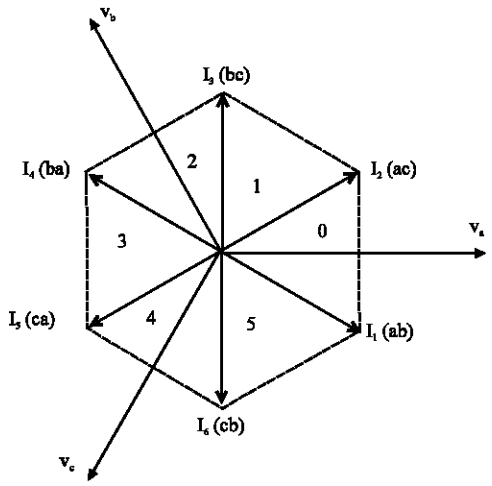

Fig. 6: Rectifier current hexagon

The modulation index m_C is often chosen to be 1, as no amplitude control of the current is desired. The calculated duty cycles can then be multiplied with the switch matrix to calculate the mean value of the input currents and the dc-link voltage as shown in Eq. (26) and (27). The switch states S_x are replaced by the vectors shown on Fig. 7 for an angle between -30° and +30°.

$$\begin{bmatrix} i_a \\ i_b \\ i_c \end{bmatrix} = d_\gamma . I_1 + d_\delta . I_2 = \left(d_\gamma \begin{bmatrix} 1 & 0 \\ 0 & 1 \\ 0 & 0 \end{bmatrix} + d_\delta . \begin{bmatrix} 1 & 0 \\ 0 & 0 \\ 0 & 1 \end{bmatrix} \right) . \begin{bmatrix} I_{DC+} \\ I_{DC-} \end{bmatrix} \quad (26)$$

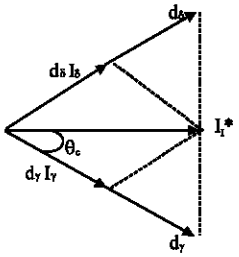

Fig. 7: Synthesis of references vector current (m = 1)

$$\begin{bmatrix} V_{DC+} \\ V_{DC-} \end{bmatrix} = \left(d_\gamma . \begin{bmatrix} 1 & 0 & 0 \\ 0 & 1 & 0 \end{bmatrix} + d_\delta . \begin{bmatrix} 1 & 0 & 0 \\ 0 & 0 & 1 \end{bmatrix} \right) . \begin{bmatrix} v_a \\ v_b \\ v_c \end{bmatrix} \quad (27)$$

From the Dc-link voltage, the output voltage can be calculated and the modulation function for the inverter can be derived.

Space vector modulation for the inverter stage: The output voltages can be found as the virtual dc-link voltages multiplied by the switch state of the inverter and at the same time the dc-link current can be found by using the transposed matrix as seen in Eq. (28) and (29).

$$\begin{bmatrix} V_A \\ V_B \\ V_C \end{bmatrix} = \begin{bmatrix} S_7 & S_8 \\ S_9 & S_{10} \\ S_{11} & S_{12} \end{bmatrix} . \begin{bmatrix} V_{DC+} \\ V_{DC-} \end{bmatrix} \quad (28)$$

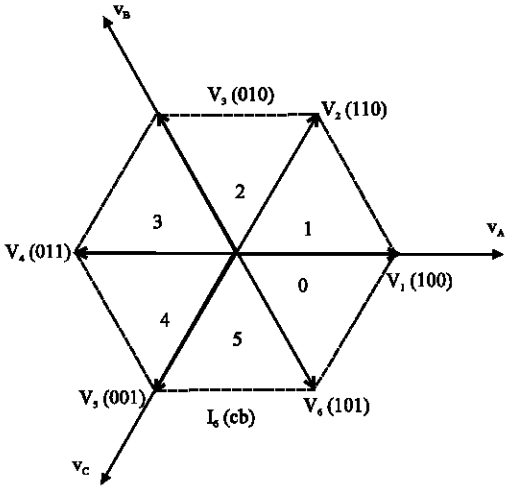

Fig. 8: Inverter voltage hexagon

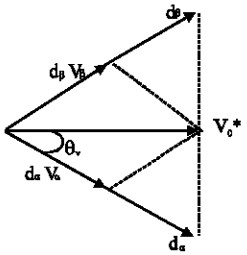

Fig. 9: Synthesis of referecne vector voltage ($m_v = 1$)

$$\begin{bmatrix} I_{DC+} \\ I_{DC-} \end{bmatrix} = \begin{bmatrix} S_7 & S_9 & S_{11} \\ S_8 & S_{10} & S_{12} \end{bmatrix} \cdot \begin{bmatrix} i_A \\ i_B \\ i_C \end{bmatrix} \quad (29)$$

Figure 8 shows the vectors that the output inverter can form by applying the dc-link voltage to the output terminals. Table 2 shows the possible switch states and the resulting length and direction of the vector. Looking at one sector, the span of the vector and the output voltage relationship shown on Fig. 9 can be found.

By geometric considerations the duty cycles can be calculated as shown in Eq. (30). By projecting the V_{out} vector on to the $V_\alpha$and V_β vectors.

$$\begin{cases} d_a = m_v.\sin\left(\frac{\pi}{3} - \theta_v\right) = T_\alpha / T_S \\ d_\beta = m_v.\sin(\theta_v) = T_\beta / T_S \\ d_{0V} = 1 - d_\alpha + d_\beta = T_{0V} / T_S \end{cases} \quad (30)$$

$$m_v = \frac{\sqrt{3}.V_O^*}{V_{DC}},\ 0 \le m_v \le 1,\ \ \theta_v = (\omega_v.t)_{mod(\pi/3)}$$

From the duty cycles, the mean value of the output voltages and the Dc-link current can be written as shown in Eq. (31) and (32).

$$\begin{bmatrix} v_A \\ v_B \\ v_C \end{bmatrix} = d_\alpha.V_6 + d_\beta.V_1 = \left(d_\alpha.\begin{bmatrix} 1 & 0 \\ 0 & 1 \\ 1 & 0 \end{bmatrix} + d_\beta.\begin{bmatrix} 1 & 0 \\ 0 & 1 \\ 0 & 1 \end{bmatrix} \right) \quad (31)$$

$$\begin{bmatrix} I_{DC+} \\ I_{DC-} \end{bmatrix} = \left(d_\alpha.\begin{bmatrix} 1 & 0 & 1 \\ 0 & 1 & 0 \end{bmatrix} + d_\beta.\begin{bmatrix} 1 & 0 & 0 \\ 0 & 1 & 1 \end{bmatrix} \right).\begin{bmatrix} i_A \\ i_B \\ i_C \end{bmatrix} \quad (32)$$

Now, when the modulation functions for both the rectifier and the inverter have been expressed, the combined modulation function can be built.

$$\begin{bmatrix} v_A \\ v_B \\ v_C \end{bmatrix} = \left(d_\alpha \begin{bmatrix} 1 & 0 \\ 0 & 1 \\ 1 & 0 \end{bmatrix} + d_\beta \begin{bmatrix} 1 & 0 \\ 0 & 1 \\ 0 & 1 \end{bmatrix} \right). \left(d_\gamma \begin{bmatrix} 0 & 1 & 0 \\ 1 & 0 & 0 \end{bmatrix} + d_\lambda \begin{bmatrix} 0 & 0 & 1 \\ 1 & 0 & 0 \end{bmatrix} \right).\begin{bmatrix} V_a \\ V_b \\ V_c \end{bmatrix} \quad (33)$$

$$\begin{bmatrix} v_A \\ v_B \\ v_C \end{bmatrix} = \left(\begin{matrix} d_\gamma d_\alpha \begin{bmatrix} 0 & 1 & 0 \\ 1 & 0 & 0 \\ 0 & 1 & 0 \end{bmatrix} + d_\lambda d_\alpha \begin{bmatrix} 0 & 1 & 0 \\ 1 & 0 & 0 \\ 1 & 0 & 0 \end{bmatrix} \\ + d_\gamma d_\beta \begin{bmatrix} 0 & 0 & 1 \\ 1 & 0 & 0 \\ 0 & 0 & 1 \end{bmatrix} + d_\gamma d_\beta \begin{bmatrix} 0 & 0 & 1 \\ 1 & 0 & 0 \\ 1 & 0 & 0 \end{bmatrix} \end{matrix} \right) \cdot \begin{bmatrix} V_a \\ V_b \\ V_c \end{bmatrix} \quad (34)$$

For the remaining time of a switch period, zero vector is applied, circulating output currents and disconnecting input voltages.

The duty cycles equation can now be written as shown in Eq. (35).

Table 2: Switch states and generated vectors for the inverter

Type	Vecteurs	$\begin{bmatrix} S_7 & S_9 & S_{11} \\ S_8 & S_{10} & S_{12} \end{bmatrix}^T$	v_A / v_{AB}	v_B / v_{AC}	v_C / v_{CA}	$\lvert V_0\rvert$	$<V_0$	I_{DC}
		$2/3V_{DC}$	$1/3V_{DC}$	$-1/3V_{DC}$				
Actifs	$V_1[1\ 0\ 0]$	$\begin{bmatrix} 1 & 0 & 0 \\ 0 & 1 & 1 \end{bmatrix}^T$	V_{DC}	0	V_{DC}	$2/3V_{DC}$	0	i_A
	$V_2[1\ 1\ 0]$	$\begin{bmatrix} 1 & 1 & 0 \\ 0 & 0 & 1 \end{bmatrix}^T$	$1/3V_{DC}V_{DC}$	$1/3V_{DC}$	$-2/3V_{DC}$			
			0	V_{DC}	$-V_{DC}$	$2/3V_{DC}$	$\pi/3$	$-i_C$
	$V_3[0\ 1\ 0]$	$\begin{bmatrix} 0 & 1 & 0 \\ 1 & 0 & 1 \end{bmatrix}^T$	$-1/3V_{DC}$	$2/3V_{DC}$	$-1/3V_{DC}$			
			$-V_{DC}$	V_{DC}	V_{DC}	$2/3V_{DC}$	$2\pi/3$	i_B
	$V_4[0\ 1\ 0]$	$\begin{bmatrix} 0 & 1 & 1 \\ 1 & 0 & 0 \end{bmatrix}^T$	$-2/3V_{DC}$	$1/3V_{DC}$	$1/3V_{DC}$			
			$-V_{DC}$	0	V_{DC}	$2/3V_{DC}$	π	$-i_A$
	$V_5[0\ 1\ 1]$	$\begin{bmatrix} 0 & 0 & 1 \\ 1 & 1 & 0 \end{bmatrix}^T$	$-1/3\ V_{DC}$	$-1/3V_{DC}$	$2/3V_{DC}$			
			0	0	V_{DC}	$2/3V_{DC}$	$-2\pi/3$	i_C
	$V_6[0\ 0\ 1]$	$\begin{bmatrix} 1 & 0 & 1 \\ 0 & 1 & 0 \end{bmatrix}^T$	$1/3\ V_{DC}$	$1/3V_{DC}$	$1/3V_{DC}$			
			V_{DC}	V_{DC}	0	$2/3V_{DC}$	$.\pi/3$	$-i_B$
Nuls	$V_0[0\ 0\ 0]\ V_7[1\ 1\ 1]$	$\begin{bmatrix} 0 & 0 & 0 \\ 1 & 1 & 1 \end{bmatrix}^T \begin{bmatrix} 1 & 1 & 1 \\ 0 & 0 & 0 \end{bmatrix}^T$				0	0	0

$$\begin{cases} d_{\alpha\gamma} = d_a.d_\gamma = m_v.\sin\left(\frac{\pi}{3}-\theta_v\right).\sin\left(\frac{\pi}{3}-\theta_C\right) = T_{\alpha\gamma}/T_s \\ d_{\alpha\delta} = d_\alpha.d_\delta = m_v.\sin\left(\frac{\pi}{3}-\theta_v\right).\sin(\theta_c) = T_{\alpha\delta}/T_s \\ d_{\beta\gamma} = d_\beta.d_\gamma = m_v.\sin(\theta_v).\sin\left(\frac{\pi}{3}-\theta_C\right) = T_{\beta\gamma}/T_s \\ d_{\beta\delta} = d_\beta.d_\delta = m_v.\sin(\theta_v).\sin(\theta_C) = T_{\beta\delta}/T_s \\ d_0 = 1-(d_{\alpha\gamma}+d_{\alpha\delta}+d_{\beta\gamma}+d_{\beta\delta}) = T_0/T_s \end{cases} \quad (35)$$

Active and reactive power control exchanged between the aerogenerator and the grid: When the DFIG is connected to an existing grid, this connection is done in three stages. The first stage is the adjustment of the stator voltages with the voltages of the grid as a reference. The second stage is the connection of the stator to the grid. While the voltages of the two devices are synchronized, this connection can be made without problem. Once this connection is carried out, the third stage is the adjustment of powers forwarded between the DFIG and the grid (Fig. 10).

By choosing a diphasic reference frame d-q related to the stator spinning field pattern and by aligning the stator vector flux Φ_s with the axis d, we can write (Aouzellag *et al*., 2006).

$$\begin{cases} \varphi_{ds} = \Phi_s \\ \varphi_{qs} = 0 \end{cases} \quad (36)$$

The Eq. (12) become then:

$$T_{em} = -P\frac{L_m}{L_s} i_{qr}\Phi_s \quad (37)$$

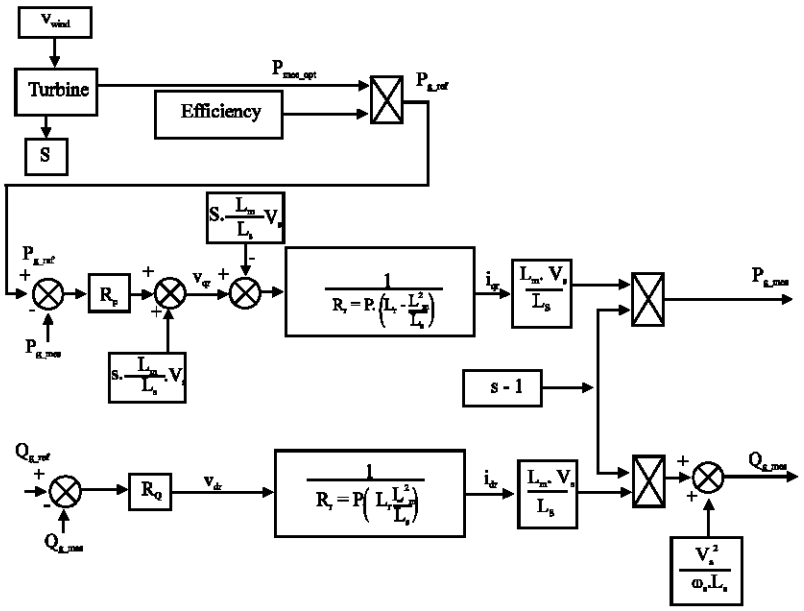

Fig. 10: Block diagram of DFIG power control

By neglecting R_s per phase stator resistance, we can then write:

$$\begin{cases} v_{ds} = 0 \\ v_{qs} = V_s \end{cases} \quad (38)$$

While, aligning itself on the reference mark chosen, we can simplify the voltages equations and stator flux as:

$$\begin{cases} v_{ds} = 0 \quad ; \; v_{qs} = V_s = \omega_s \Phi_s \\ \varphi_{ds} = \Phi_s = L_s i_{qs} + L_m i_{qr} \quad ; \; \varphi_{dr} = L_r i_{dr} + L_m i_{ds} \\ \varphi_{qs} = 0 = L_s i_{ds} + L_m i_{dr} \; ; \; \varphi_{qr} = L_s i_{qr} + L_m i_{qs} \end{cases} \quad (39)$$

The following expressions for the active and reactive stator powers are given by:

$$\begin{cases} p_s = - V_s \dfrac{L_m}{L_s} i_{qr} \\ Q_s = \dfrac{V_s \Phi_s}{L_s} - \dfrac{V_s L_m}{L_s} i_{dr} \end{cases} \quad (40)$$

The expressions of the rotor voltages become:

$$\begin{cases} v_{dr} = R_r i_{dr} + \left(L_r - \dfrac{L_m^2}{L_s} \right) \dfrac{di_{dr}}{dt} - s.\omega_s \left(L_r - \dfrac{L_m^2}{L_s} \right) i_{qr} \\ v_{qr} = R_r i_{qr} + \left(L_r - \dfrac{L_m^2}{L_s} \right) \dfrac{di_{qr}}{dt} + s.\omega_s \left(L_r - \dfrac{L_m^2}{L_s} \right) i_{dr} + s \dfrac{L_m . V_s}{L_s} \end{cases} \quad (41)$$

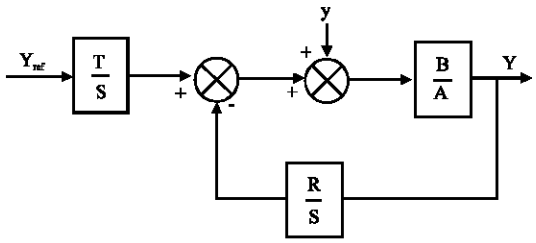

Fig. 11: Block diagram of the RST controller

With

$$s = \frac{\omega_s - \omega}{\omega_s} \quad (42)$$

The expressions of the powers exchanged between the DFIG and the grid become

$$\begin{cases} P_g = (s-1) V_s . \dfrac{L_m}{L_s} . i_{qr} \\ Q_g = \dfrac{V_s^2}{\omega_s . L_s} + (s-1) V_s \dfrac{L_m}{L_s} i_{dr} \end{cases} \quad (43)$$

The active reference power is determined by the following expression:

$$P_{g\_ref} = -\eta . P_{mec\_opt} \quad (44)$$

With η is the efficiency of the DFIG

The blocks R_p and R_Q represent active and reactive power regulators. The aim of these regulators is to obtain high dynamic performances in terms of reference tracking, sensitivity to perturbations and robustness. The RST regulator is studied and it is detailed below.

The block diagram of a system with its RST controller is shown in Fig. 11.

The system with the transfer function B/A has Y_{ref} as reference and is disturbed by the variable γ. R, S and T are polynomial which constitutes the controller. In our case, we have

$$A = L_s R_r + pL_s\left(L_r - \frac{L_m^2}{L_s}\right) \text{ and } B = L_m V_s \quad (45)$$

$$Y = \frac{BT}{AS+BR} Y_{ref} + \frac{BS}{AS+BR}\gamma \quad (46)$$

The equation characteristic of the system is

$$D = AS + BR = CF \quad (47)$$

Where C is the command polynomial and F is the filtering polynomial. In order to have good adjustment accuracy, we choose a strictly proper regulator. So if A is a polynomial of n degree we must have

$$\deg(D) = 2n+1$$
$$\deg(S) = \deg(A)+1$$
$$\deg(R) = \deg(A)$$

In our case

$$\begin{cases} A = a_1 p + a_0 & ; \ B = b_0 \\ R = r_1 p + r_0 & ; \ S = s_2 p^2 + s_1 p + s_0 \\ D = d_3 p^3 + d_2 p^2 + d_1 p + a_0 \end{cases} \quad (48)$$

To find the coefficient of polynomial R and S, the robust pole placement method is adopted.

RESULTS AND DISCUSSION

We present the dynamic simulation of the behaviour of the studied aerogenerator. The control of powers exchanged between the wind turbine and the grid is carried out by the low directed control lever. The shown results are obtained with a reactive power of reference $Q_{g\_ref} = 0$ and $P_{g\_ref} = -\eta . P_{mec\_opt}$.

The wind velocity is represented by Fig. 12 and that of the slip by Fig. 13 which is wind velocity image and varies from -0.3 to +0.3. Figure 14 represent the mechanical

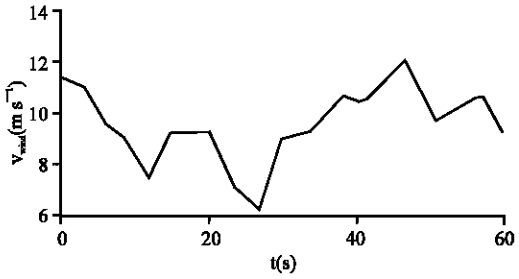

Fig. 12: Wind speed

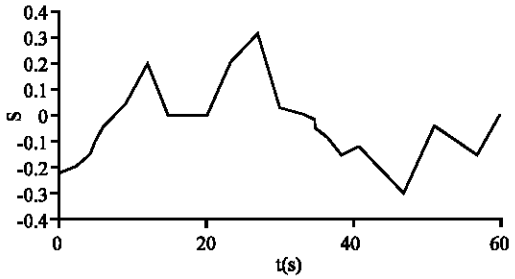

Fig. 13: DFIG slip

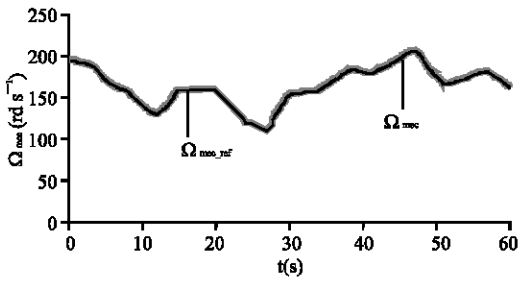

Fig. 14: Generator mechanical speed

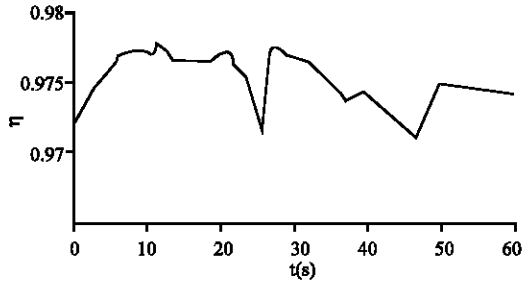

Fig. 15: DFIG efficiency

speed which is the slip image. The output pace of the generator is shown by Fig. 15; this last varies between 97 and 98% that justifies that the power losses are reduced in the high level powers machines. Figure 16 represents the optimal mechanical power absorbed by the DFIG. Figure17a and b show the active and reactive powers, respectively exchanged between the rotor and the grid; their flow direction depends on the sign of the slip, for

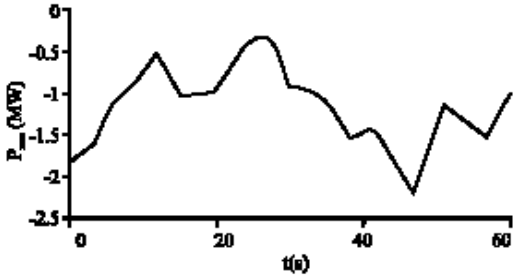

Fig. 16: Turbine mechanical power

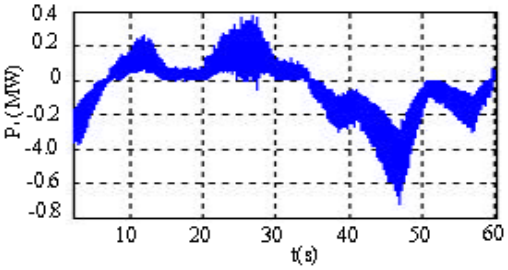

Fig. 17a: Rotor active power

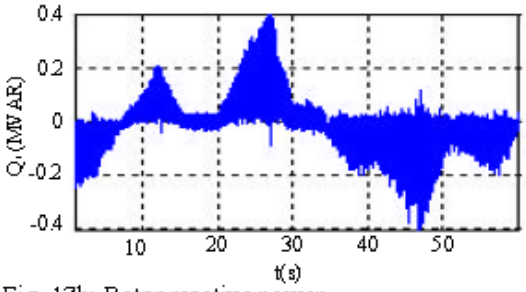

Fig. 17b: Rotor reactive power

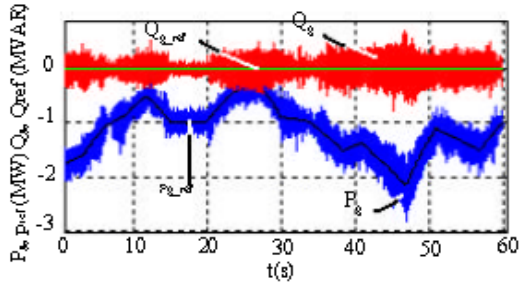

Fig. 18: Grid active and reactive powers

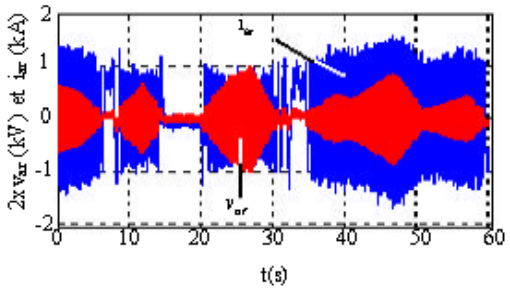

Fig. 19a: Rotor voltage and current

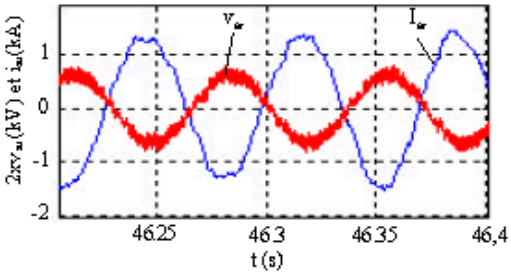

Fig. 19b: Rotor voltage and current (s<0)

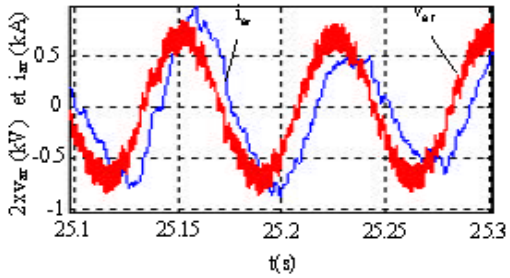

Fig. 19c: Voltage and current (s>0)

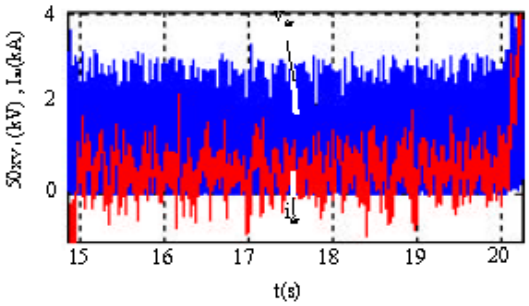

Fig. 19d: Voltage and current (s = 0)

(s<0) the powers are transmitted rotor to the grid (DFIG operates in super-synchronous), for (s>0) the powers are transmitted from the to the rotor (DFIG operates in sub-synchronous) and for a zero slip the rotor absorbs an active power of about 2% of the stator nominal output and the reactive power is null. Figure 18 shows the powers exchanged between the wind turbine and the grid which follow perfectly the reference scales and we notice that the active power is transmitted from the aerogenerator to the grid and this for the three operating modes. Figure 19a shows the voltage and the rotor current, Fig. 19b zoom rotor tension and current (s<0) (the current is behindhand to the voltage from an angle of$\varphi>\pi/2$) and Fig. 19c zoom voltage and current (s>0) (the dephasing angle between voltage and current $\varphi<\pi/2$),

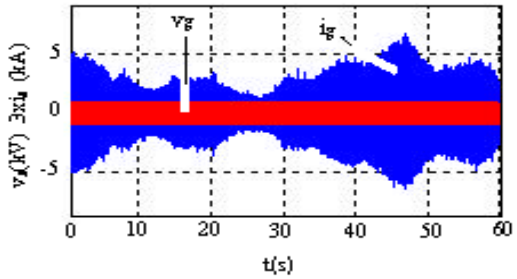

Fig. 20a: Gride voltage and current

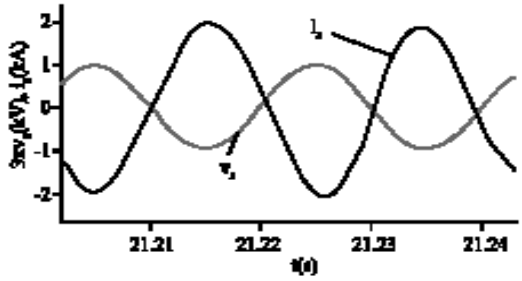

Fig. 20b: Gride voltage and current

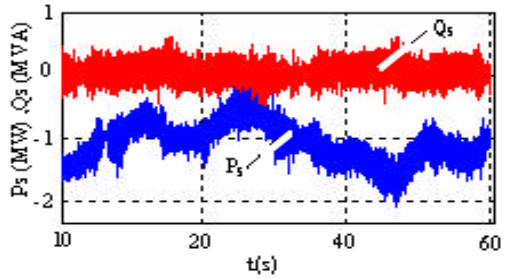

Fig. 21: Stator active and reactive power

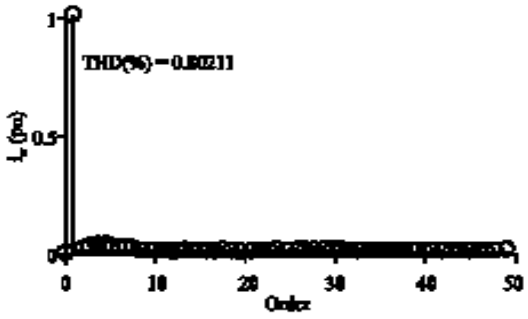

Fig. 22: Rotor current spectre

Fig. 20a has shown that the voltage is imposed by the grid and the current amplitude injected to the grid varies according to the slip and the zoom voltage running shows that the latter are in opposition of phase for all the operating modes (the system provides power to the grid)

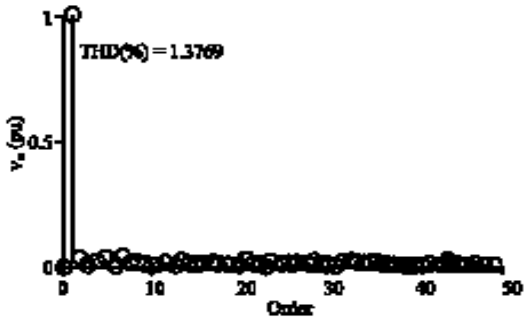

Fig. 23: Rotor voltage spectre

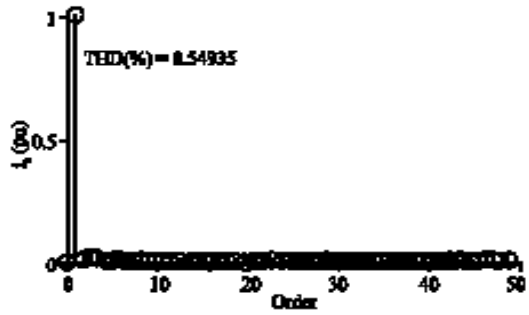

Fig. 24: Gride current spectre

(Fig. 20b). Figure 21 represents the stator active and reactive powers and that active and of negative sign that justifies that this stator power is transmitted to grid. The spectre analysis of voltage and current shows in Fig. 22-24, illustrate the high quality of the obtained signal.

CONCLUSION

The research presented in this article is devoted to the analysis, modelling and simulation of an aerogenerator with variable speed based on a double fed asynchronous machine controlled by the rotor using a matrix converter. The power control of the machine is carried out by the technique of directed flow control lever. The results of simulation presented show that the DFIG functions in the two couple-speed quadrants in generating mode sub-synchronous and super-synchronous. For a zero slip, the DFIG functions as synchronized asynchuonous generator and the rotor is supplied by continuous scales. The active power provided to the grid varies according to the wind velocity and follows the power of reference that justifies that the power injected in the grid is that recovered by the application of MPPT algorithm. Work is on hand in order to associate the studied system with storage of energy in the inertial form allowing operation either on a grid or on isolated loads.

Appendix

Aerogenerator parameters

- $L_s = L_r = 0.0137$ H; R = 36.5 m
- $L_m = 0.0135$ H; G = 124
- $R_s = 0.012\ \Omega$; f = 0.0071
- $R_r = 0.021\Omega$; J = 500 kg.m^2
- $V_s = 690$ V; P = 2

Nomenclature:

Ω_t	:	Turbine speed. (rd/s).
Ω_{mec}	:	Mechanical speed of the DFIG.
Ω_{mec_ref}	:	Mechanical speed reference.
P_{mec_opt}	:	Mechanical Optimal.
T_{aero}	:	Aerodynamic torque.
T_g	:	Generator torque.
s	:	Generator slip.
C_p	:	Power coefficient.
λ	:	Tip speed ratio.
ρ	:	Air density.
R	:	Turbine radius.
v_{wind}	:	Wind velocity.
G	:	Gear ratio.
η	:	DFIG efficiency.
v_{ds}, v_{qs}, v_{dr}, v_{qr}	:	Two-phase stator and rotor voltages.
ϕ_{ds}, ϕ_{qs}, ϕ_{dr}, ϕ_{qr}	:	Two-phase stator and Rotor fluxes.
i_{ds}, i_{qs}, i_{dr}, i_{qr}	:	Two-phase stator and rotor currents.
R_s, R_r	:	Per phase stator and rotor resistances.
L_s, L_r	:	Total cyclic stator and rotor inductances.
L_m	:	Magnetizing inductance.
P	:	Number of pole pairs.
J	:	Inertia.
f	:	Viscous friction.
p	:	Laplace operator.
P_s, Q_s	:	Active and reactive power.
P_r, Q_r	:	Rotor active and reactive power.
P_{g_ref}, Q_{g_ref}	:	Reference of DFIG active and reactive power.
P_g, Q_g	:	Active and reactive gride power.
v_a, v_b, v_c	:	Input phase voltages.
i_A, i_B, i_C	:	Output phase currents.
i_a, i_b, i_c	:	Input phase currents.
S_{ij}	:	Function switch.
T_s	:	Switching interval.
θ_i	:	Angle of the reference input current vector.
θ_o	:	Angle of the reference output current vector.

REFERENCES

Alesina, A. and M. Venturini, 1988. Intrinsic amplitude limits and optimum design of switches direct PWM ac converter. Proc. PSEC Conf. Rec., pp: 1284-1290.

Aouzellag, D., K. Ghedamsi and E.M. Berkouk, 2006. Modelling of Doubly Fed Induction Generator with Variable Speed Wind Turbine for Network Power Flow Control. Wseas Trans. Power Syst., ISSN 1790-5060, 1(2): 1995-2000.

Chang, L., 2002. Systèmes de conversion de l'énergie éolienne. IEEE. Can. Rev., pp: 1-5.

Chang, L., 2002. Systemes de conversion de l'énergie éolienne. IEEE. Can. Rev., pp: 1-5.

El Aimani, S., 2003. Modelling and simulation of doubly fed induction generator for variable speed wind turbines integrated in a distribution network. In: 10th European conference on power electronics and application. Toulouse, France.

Ghedamsi, K., D. Aouzellag and E.M. Berkouk, 2006. Application of matrix converter for variable speed wind turbine driving a doubly fed induction generator. SPEEDAM, IEEE Xplore, pp: S3- 38-42.

Han Ju Cha, 2004. Analysis and design of matrix converter for adjustable speed drives and distributed power sources. PHD Thesis, Texas A and M University.

Poitier, F., 2003. Etude and commande de génératrices asynchrone pour l'utilisation éolienne. Thèse de Doctorat, Université de Nantes.

Poitiers, F. *et al.*, (N.D). Control of a doubly fed induction generator for wind energy conversion systems. GE44-LARGE. Saint Nazaire, France.

Robyns, B. and M. Nasser, 2001. Modélisation et simulation d'une éolienne à vitesse variable basée sur une génératrice asynchrone à cage, in the Proceeding of Electrotechnique du Futur EF, Nancy, France, pp: 77-82.

Taraft, S., D. Rekioua and D. Aouzellag, 2007. Etude des performances de la MADA dans une éolienne à vitesse variable connectée au réseau. ICRE University of Bejaia, pp: 1-6.